AIP | Review of Scientific Instruments

Performance of a short "magnetic bottle" electron spectrometer

M. Mucke, M. Förstel, T. Lischke, T. Arion, A. M. Bradshaw, and U. Hergenhahn

Citation: Review of Scientific Instruments **83**, 063106 (2012); doi: 10.1063/1.4729256
View online: http://dx.doi.org/10.1063/1.4729256
View Table of Contents: http://scitation.aip.org/content/aip/journal/rsi/83/6?ver=pdfcov
Published by the AIP Publishing

Performance of a short "magnetic bottle" electron spectrometer

M. Mucke,[1,a)] M. Förstel,[1,2] T. Lischke,[1,b)] T. Arion,[1,c)] A. M. Bradshaw,[1,3] and U. Hergenhahn[4,d)]
[1]*Max-Planck-Institut für Plasmaphysik, EURATOM Association, Boltzmannstr. 2, 85748 Garching, Germany*
[2]*Max-Planck-Institut für Kernphysik, Saupfercheckweg 1, 69117 Heidelberg, Germany*
[3]*Fritz-Haber-Institut der Max-Planck-Gesellschaft, Faradayweg 4-6, 14195 Berlin, Germany*
[4]*Max-Planck-Institut für Plasmaphysik, EURATOM Association, Teilinstitut Greifswald, Wendelsteinstr. 1, 17491 Greifswald, Germany*

(Received 19 April 2012; accepted 25 May 2012; published online 14 June 2012)

In this article, a newly constructed electron spectrometer of the magnetic bottle type is described. The instrument is part of an apparatus for measuring the electron spectra of free clusters using synchrotron radiation. Argon and helium outer valence photoelectron spectra have been recorded in order to investigate the characteristic features of the spectrometer. The energy resolution ($E/\Delta E$) has been found to be ~30. Using electrostatic retardation of the electrons, it can be increased to at least 110. The transmission as a function of kinetic energy is flat, and is not impaired much by retardation with up to 80% of the initial kinetic energy. We have measured a detection efficiency of most probably $0.6^{+0.05}_{-0.1}$, but at least of 0.4. Results from testing the alignment of the magnet, and from trajectory simulations, are also discussed. [http://dx.doi.org/10.1063/1.4729256]

I. INTRODUCTION

In photoelectron spectroscopy, it is desirable for a number of experiments to maximize the solid angle under which electrons are collected. In particular this might be the case for coincidence experiments, in which a primary photoelectron is to be detected together with a secondary electron produced in the same event, and for experiments on ultra-dilute targets, such as free ion beams. For gaseous targets, several methods have been established for the energy-resolved collection of electrons under solid angles of up to 4π sr, each offering various advantages and disadvantages. Without going into any detail, we would like to mention cold target recoil ion momentum spectroscopy,[1] and velocity map imaging.[2] Yet another type of instrument uses a magnetic field configuration, originally investigated in plasma physics,[3] to collect and guide electrons onto a detector, and has become known as the magnetic bottle spectrometer.[4] In our group we have built a magnetic bottle spectrometer for electron spectroscopy on a free cluster jet after ionization by synchrotron radiation. In particular, we are interested in autoionization processes induced by fast intra-cluster energy transfer, such as intermolecular Coulombic decay.[5] For the unambiguous detection of such processes, but also for other studies in cluster photoionization,[6] the excellent detection efficiency of this instrument even for very low energy electrons has proven to be invaluable. In this paper we describe the construction of our instrument. This is followed by a detailed report of its performance, in particular the transmission as a function of kinetic energy, and the energy resolution. The influence of static electric (retardation) fields on the detection efficiency and the resolution is described. We have also investigated source size effects by ray-tracing simulations as well as in actual experiments.

A magnetic bottle type electron spectrometer basically is an electron time-of-flight spectrometer in which additional magnetic fields dramatically increase the collection efficiency, while still covering the full kinetic energy range in a single measurement. Two different magnetic fields are used in the spectrometer: a strong and inhomogeneous field covering the interaction region and a weak homogeneous magnetic field to guide the collected electrons along a drift tube. When looking at the resulting field lines, the name of the spectrometer becomes obvious: they exhibit the shape of a bottleneck. In the words of Kruit and Read,[7] the design of the spectrometer is based on the principle that "a diverging magnetic field has the property of aligning the trajectories of electrons that travel from the strong field region to the weak field region." The theory of operation of a magnetic bottle spectrometer has been made very transparent in earlier papers,[4,8] and we will not repeat these derivations here. The basic idea used to increase the collection efficiency is the following: electrons are produced in a region of a strong magnetic field, pointing, say, into the z direction. The field is inhomogeneous in such a way that its absolute strength decreases for larger z values. The free electrons will then spiral around the magnetic field lines, but due to the field gradient their movement will be guided into the positive z direction. Because the movement of electrons in a magnetic field is energy conserving, and the angular momentum of the motion around the field lines must similarly be conserved, the movement of the electrons is parallelized to follow the field lines also in the region of weak magnetic field. This weak magnetic field, produced by a field coil, extends over a length that can be up to several meters. At the end of

a)Present address: Department of Physics and Astronomy, Uppsala University, Box 516, 751 20 Uppsala, Sweden.
b)Present address: Fritz-Haber-Institut der Max-Planck-Gesellschaft, Faradayweg 4-6, 14195 Berlin, Germany.
c)Present address: Institut für Experimentalphysik, Universität Hamburg, Luruper Chaussee 149, 22761 Hamburg, Germany.
d)E-mail address: uwe.hergenhahn@ipp.mpg.de. Mail address: Helmholtz-Zentrum Berlin, Albert-Einstein-Str. 15, 12489 Berlin, Germany.

this drift region the electrons are collected by microchannel plates. Their original kinetic energy can be calculated from their time-of-flight. That said, it is clear that magnetic bottle spectrometers can only be used with pulsed sources of ionization with repetition rates not much higher than the total time-of-flight of electrons in the instruments, typically in the range of 1–10 μs. This includes many lasers and free electron lasers, but also synchrotron radiation when the storage ring is operated in a mode with only a few circulating bunches.

The magnetic field configuration outlined above was originally investigated as a photoemission microscope (and indeed it is important that the magnetic field lines lead to a point-to-point mapping of the interaction region onto the detector).[9] Kruit and Read were the first to report on such a magnetic field-assisted time-of-flight spectrometer for gas phase photoelectron spectroscopy.[4] They demonstrated that the collection efficiency could dramatically be increased while maintaining an energy resolution which is sufficient for many experiments. With an electromagnet, originally used in transmission electron microscopy, they generated an inhomogeneous magnetic field of $B_i = 1$ T at the source point of photoelectrons, which in their experiment were created by multi-photon laser ionization of rare gas atoms. A solenoid of 0.5 m length connected this interaction region with the detector, presenting a weak and homogeneous magnetic field ($B_f = 1$ mT) region the electrons had to pass. A typical value achieved for the energy resolution in this first instrument was 70 meV for electrons of 1.93 eV kinetic energy E, or a $E/\Delta E$ of 27.5.

Since the pioneering work of Kruit and Read, numerous magnetic bottle spectrometers have been developed in various groups, adapted to the specific needs of each experiment and to the technical possibilities available at that time. Most of the developments were concerned with the production of the strong magnetic field which determines the design of the interaction region. Tsuboi *et al.*[8] made use of permanent magnets to create the inhomogeneous magnetic field, which leads to added flexibility in the design of the interaction region. Cheshnovsky *et al.* introduced changes to the geometry of those magnets and noted that the angular acceptance can be increased from 2π sr, (Refs. 4 and 8) to almost 4π sr by placing the interaction region a small distance away from the point of maximum field strength, in the direction of the detector.[10] Electrons which are originally emitted away from the detector are thus "turned around" when they try to enter the region of highest B-field ("magnetic mirror"). Only electrons the trajectories of which are directed (almost) parallel to the B-field lines and away from the detector cannot be turned around. The use of a magnetic bottle spectrometer for electron-electron coincidence spectroscopy has been pioneered by Eland *et al.*[11] using a laboratory light source and, at almost the same time, by Lablanquie *et al.* using synchrotron radiation.[12] This work has been continued by the groups of Penent and Feifel, and thanks to the good collection efficiency of magnetic bottle spectrometers, Lablanquie *et al.* were recently able to show the existence of two-site double core holes in small molecules.[13]

The versatility of the magnetic bottle spectrometer concept is shown by the diverse list of other experiments in which this type of instrument has been used. Some examples are (time-resolved) laser spectroscopy on molecules,[14] clusters,[15–17] molecular and cluster anions[10,18] and even liquid beams,[19] but also positron annihilation spectroscopy.[20] In recent years, the potential of using magnetic bottles also at free electron lasers has been recognized and first experiments have been performed.[21] The instrument described here has also been used for the study of laser photoionization of a fast beam of molecular anions.[22]

II. DESIGN OF THE INSTRUMENT

As mentioned in the Introduction, a magnetic bottle electron spectrometer essentially consists of two parts: an interaction region characterized by a strong, inhomogeneous magnetic field, and a drift tube of low and homogeneous magnetic field at the end of which a detector is placed. For the magnetic bottle-type electron energy analyzer presented here, we have adapted the design of Lablanquie *et al.*[12,23] To give a visual impression, the layout is sketched in Fig. 1. Similar to

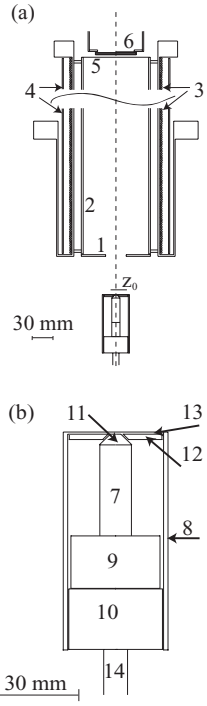

FIG. 1. (a) Schematic drawing of the spectrometer (to scale). The magnet set-up can be aligned relative to the drift tube by an xyz-manipulator. It is placed close to the interaction region (at z_0). Opposite the magnet and 45 mm away from the interaction region is the entrance aperture (1) (25 mm in diameter) of the drift tube (2). The drift tube has an inner diameter of 85 mm and a length of 600 mm. It is terminated by a copper mesh (5), behind which the detector, an MCP double stack of 42 mm active area plus a phosphor screen (6), is mounted. Around the drift tube but outside of the vacuum, a copper coil is wound for ~270 turns, creating a solenoid of 110 mm diameter (3). The solenoid is covered by a Mu-metal shield (4). (b) The permanent magnet and magnet holder in detail: The magnet (7) is topped by a soft iron cone (11) and has a soft iron base (9) at the opposite end. The PEEK (polyether ether ketone) spacer (10) serves as an electrically insulated mounting of the magnet. The potential plate (aluminum, 12) and the mesh (13) in front of the magnet allow the application of electric fields. (8) is a PEEK holder and (14) the connection with the xyz-manipulator. Threads connecting (9) to (10) and (14) to (10) are not drawn.

older designs, we have chosen to produce the strong and inhomogeneous field of our spectrometer by a permanent magnet. Compared to the use of an electromagnet, less space is needed, which in turn allows for more freedom in the design of the interaction region. For example, in our set-up we have placed a skimmer to select the central part of our cluster jet at close distance. Focusing properties and collection efficiency of the spectrometer can be adjusted by varying the distance of the magnet tip to the interaction region with the help of an xyz-manipulator, as will be discussed below.

In order to create the strongest magnetic field possible in a confined geometry, a soft iron cone (45° angle at the base) has been placed on top of the magnet. It has been matched with a soft iron base at the opposite end of the magnet, so that the field lines are efficiently guided through. The support of the magnet has been designed in such a way that allows the use of magnets with different diameter in the same set-up. For the measurements presented here, three Sm_2Co_{17} magnets of 10 mm diameter and a length of 10 mm each have been used. The soft iron cone had a tip diameter of 3.1 mm. The field strength achieved was 450 mT at the tip of the cone, corresponding to ∼200 mT in the interaction region, which is a few mm away from the tip. Magnets produced for industrial purposes were employed (IBS Magnete, Berlin).

The spatial distribution of the magnetic field has been measured with a Hall probe. Within a circle of 2.5 mm radius the z component of the magnetic field dropped to 50%–60% of its maximal value. This shows that the soft iron cone indeed bundles the field lines. The general shape of the field deviates from the expected radial symmetry. Rather the components of the field lines within the xy-plane (small, compared to the z component) showed a propensity to align along one axis. We have not investigated other magnet specimen, but the existing result in our opinion shows that the shape of the B field should not be taken for granted when industrial magnets are used.

Opposite the magnet, the drift tube is mounted with the detector at its other end. The length of the drift tube was adapted to the single bunch repetition rate of the BESSY II synchrotron radiation source in Berlin, Germany, which is 1.25 MHz. Its length is thus only 0.6 m, so that even slow electrons with a kinetic energy down to ∼1.85 eV arrive at the detector before the next ionization event takes place.

The homogeneous magnetic field is produced by a solenoid, i.e., a current of 1.0–1.2 A is sent through a lacquered copper wire with a thickness of 2 mm, which is wrapped ∼270 times around the drift tube, thus producing field strengths of ∼0.5–0.6 mT. We have found that the performance is not affected much by the exact setting of this value, although a too low guiding field (0.25 mT) may result in a kinetic energy dependence of the transmission function. The solenoid is placed outside the vacuum, which has a number of advantages, e.g., less material is inside the vacuum which may outgas, and it may be removed for baking. A wire of 2 mm diameter is used, so that Ohmic heat production in the coil is low. The solenoid is covered by 2 layers of Mu-metal foil to avoid deformation of the weak magnetic field inside the drift tube by the earth's magnetic field.

In addition to the magnetic fields, the electron velocities and focusing properties of the spectrometer can also be controlled by electric fields. For this purpose, an electrically insulated drift tube is mounted inside the solenoid. It is separated from the interaction volume by an entrance aperture of 25 mm opening at a distance of 45 mm, and is terminated by a copper mesh a few mm in front of the detector. If desired, a retarding potential (for improved energy resolution) or an accelerating potential (to collect all electrons within a given flight time) can be applied along the interaction region. Voltages on the drift tube and the entrance diaphragm can be controlled separately. In order to make the electric field distribution across the interaction region as homogeneous as possible, a copper mesh has been fixed in front of the magnet. The freedom to control three bias potentials separately (drift tube, diaphragm, mesh, magnet) can be used in various ways, not all of which have been fully explored yet. One option is to control electron optical effects when the electrons encounter a potential step at the entrance to the drift tube.[24] Another might be to bias the interaction region by applying the same voltage to all three elements, which could be used to prevent low energetic stray particles from entering the interaction region. The mesh in front of the magnet also serves another purpose, namely to electrically shield the magnet itself from the interaction region. This allows a positive bias voltage to be applied to the magnet in order to hinder secondary electrons produced on its surface from penetrating into the interaction region. This potential is also applied to the soft iron cone of the magnet, and to a small aluminum plate, which together with the cone forms a flat bias electrode. Further details of the design have been described.[25]

An alternative set-up used in some experiments consists of smaller diameter magnets (5 mm), equipped with a smaller soft iron cone, but without a mesh in front of the magnet assembly. The energy resolution of the spectrometer was not affected grossly by this exchange.

Electrons generated in an ionization event are emitted in all directions. They are captured by the field lines of the strong magnetic field and forced to follow them towards the low magnetic field region. Electrons originally emitted towards the permanent magnet will be turned around by the increasing magnetic field strength. In the transition from the region of the strong inhomogeneous field to the weak and homogeneous field, and before entering the drift tube, the electron trajectories are parallelized. Once in the solenoid, the electrons follow the parallel magnetic field lines to the detector. The latter consists of a Chevron type MCP double stack with an active area of 42 mm and an open area ratio of 60%, plus a phosphor screen. During normal operation, a voltage of ∼1900 V is applied across the MCP stack and a bias of ∼+300 V to the front MCP to provide for a pre-acceleration of the electrons and thus an increased detection efficiency. The signal of detected electrons is coupled out from the phosphor screen via a capacitance. After amplification it is fed into a constant fraction discriminator. The filtered signal is then led to a multi-hit-capable, time-to-digital converter with 60 ps bin width (GPTA, Berlin) and recorded in an event-based manner. Electron flight times t (stop signal) are measured with respect to the BESSY II bunch marker signal (start signal), and are thus determined up to a fixed, but unknown time offset t_0. Electron kinetic energies are later inferred from the measured

times-of-flight via a time-to-energy conversion, $E = -eU_{ret} + d^2/(t - t_0)^2$. The difference in effective retardation voltage between the regions outside and inside the drift tube is taken into account by breaking up the flight path into two sections, each treated separately by the above formula. d contains natural constants and the respective section length. t_0 and exact values of the retardation voltage U_{ret} (see below) are treated as adjustable parameters, to be determined from reference measurements on rare gas photoelectron lines. Imaging the electrons on the phosphor screen is possible, and routinely used for alignment purposes.

The spectrometer is part of a set-up dedicated to research on van der Waals bound clusters. This consists of an expansion chamber for cluster generation and the main chamber, which are connected via a conical skimmer (15° half opening angle, open diameter 1 mm). The interaction between sample and ionizing radiation takes place in the main chamber, where the spectrometer is mounted such that the sample beam and the synchrotron radiation beam cross each other perpendicularly in front of the magnet tip. To ensure pressures below 1×10^{-5} mbar required for microchannel plate operation, a turbomolecular pump at the detector end of the spectrometer supports the main one close to the interaction region. In this configuration, the spectrometer is mounted pointing downward, while for experiments on an ion beam it was mounted pointing upwards.[22]

In order to characterize the new spectrometer, electron time-of-flight spectra after single photon ionization of helium and argon were recorded. All measurements shown here used synchrotron radiation with a linear polarization in the storage ring plane. The spectrometer axis was oriented vertically. The BESSY II beamlines UE112/PGM-1 (result shown in Fig. 2) and TGM4 (all other results) were used. The latter was a bending magnet beamline, which originally had been constructed for BESSY I, the predecessor of BESSY II. Energy resolution and photon flux were therefore worse than expected of a third generation synchrotron radiation source (see below). Sample gas was admitted to the interaction region via our supersonic jet for production of rare gas clusters,[26] with the nozzle kept at room temperature. For the data shown in Figs. 3 and 4, gas was leaked in via a non-magnetic needle placed a few mm away from the interaction region.

Ionization energies of the He 1s and the Ar $3p_{3/2}$ levels, frequently used below, are at 24.59 and 15.76 eV, respectively.

III. RESULTS AND DISCUSSION

A. Lineshape analysis

Kruit and Read have already described the lineshapes observed with a magnetic bottle spectrometer.[4] Compared to studies with synchrotron radiation, however, this work differs in one important aspect, namely, the shape of the interaction region: Since Kruit and Read used multi-photon ionization, the interaction region in their experiment was confined to a small (10 μm diameter) region in space, on the rotational axis of the spectrometer. (To achieve the intensities necessary for a multi-photon process, their laser beam had to be focused strongly.) In contrast, in synchrotron radiation experiments,

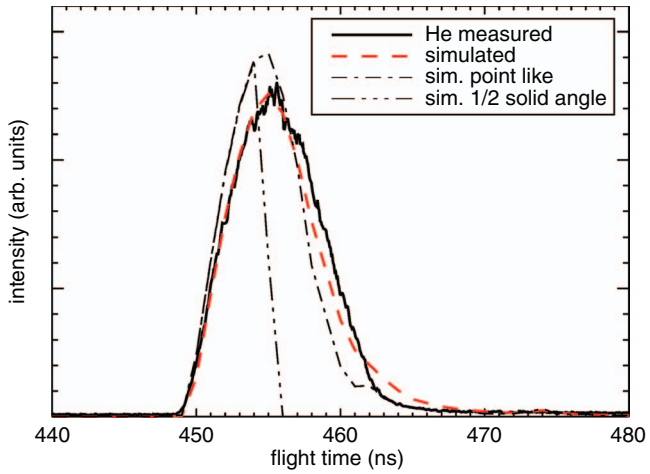

FIG. 2. Comparison of the measured time-of-flight spectrum of He 1s photoelectrons with charged particle trajectory calculations. A kinetic energy of 5 eV and an acceleration voltage of 1.1 V were chosen. The thick solid black line and the dashed lines are the measured and simulated spectra, respectively. The simulation given by the (simple) dashed line includes the effect of the finite size of the interaction region, with 3 mm extension along a line perpendicular to the spectrometer central axis, and 0.2 mm diameter in the remaining two dimensions, which is an estimate for the spatial overlap of light beam and gas jet. The other two traces were calculated under the assumption of a point-like interaction region (dash-dotted line), and under the additional restriction of admitting electron emission only into the half sphere on the drift tube side (dash-dot-dot-dotted line). The simulated traces were normalized to the same total area as the measurement (half the total area for the last trace). See text for details.

single photon ionization inevitably occurs along a line made by the intersection of the photon beam with the gas jet. The region out of which any electrons can enter the spectrometer can thus be quite extended along one dimension. Although the effect of off-center emission on the spectra has been discussed,[4] questions remain as to what extent the size of the interaction

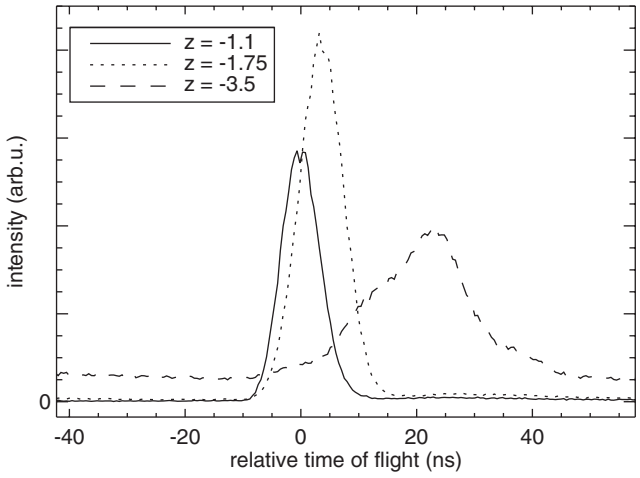

FIG. 3. He 1s time-of-flight spectra recorded at a kinetic energy of 3.4(5) eV (photon energy of 28 eV). For the solid line spectrum the magnet was placed as close to the interaction region as possible. The dotted line spectrum drawn was recorded at the z-value of the magnet which gave the maximum count rate, and the dashed line spectrum at an even larger value of z. The z axis coincides with the rotational axis of the spectrometer, and the interaction region is placed at $z = 0.0 \pm 0.1$ mm. The time-of-flight is given relative to the maximum of the $z = -1.1$ mm spectrum, because the absolute zero of the time scale for this series has not been established.

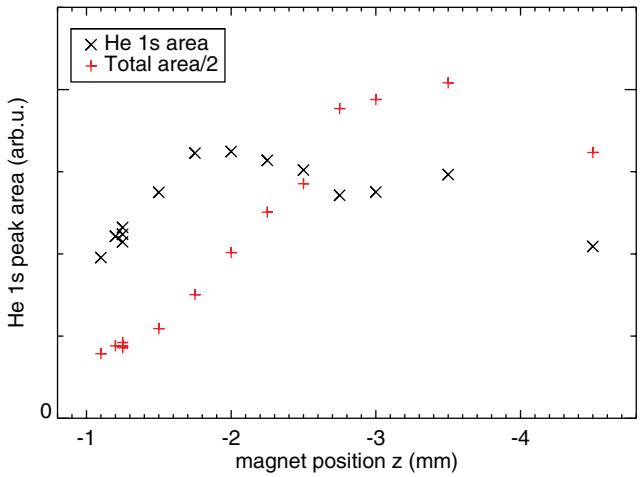

FIG. 4. Peak areas of He 1*s* spectra (crosses) recorded at a photon energy of 28 eV as a function of the distance between the permanent magnet and the interaction region. The total number of counts in each spectrum is also shown (plus signs), and has been divided by a factor of two for easier comparison.

region in synchrotron radiation experiments degrades the energy resolution, compared to the point-like case.

We have attempted to answer this question by comparing a measured spectrum to simulated ones. Simulations have been done using a programme for particle raytracing in electric and magnetic fields.[27] As magnetic fields in this programme are (most easily) introduced via a *scalar* potential,[28] we have modeled the magnetic field by two successive homogeneous fields. One strong field we have defined between the upper and lower surfaces of our permanent magnet, and one weak field inside the drift tube. The "equipotential lines" for the resulting field indeed are mimicking the field distributions that were sketched in earlier work.[4,10] For all simulations, electrons with varying source positions, take-off angles and kinetic energy were produced and propagated by raytracing.[29] Kinetic energies in all cases were modeled as a Gaussian distribution with a width being equal to the monochromator broadening. The distribution of take-off angles followed the well-known angular distribution function of photoelectrons, and included the $\sin\phi$ weighting factor which appears in the surface integral over a sphere, with ϕ being the emission angle relative to the polarization vector. Three different assumptions were made for the spatial distribution of the interaction region, and are explained below.

In Fig. 2, the time-of-flight spectrum of He 1*s* photoelectrons as obtained from ionization with 29.6 eV photons is shown (solid line). For this spectrum, the instance in which the synchrotron radiation pulse occurred was determined from the signal of scattered vacuum ultra-violet (VUV) photons. The time-of-flight axis was thus put on an absolute scale.

The measured spectrum is compared to simulations using three different sets of parameters. We focus first on the dashed line, which is intended to reproduce the measured data. For this set of simulated trajectories, a source distribution of $(0.2 \times 3.0 \times 0.2)$ mm^3 Gaussian widths, corresponding to the spatial overlap of the light beam and the gas jet, was assumed. The simulation agrees quantitatively with the measured line shape, which shows that realistic results can be obtained by our procedure despite the simplified shape of the magnetic field we have used. Times-of-flight for the same number of trajectories, but for electrons being emitted from a point-like interaction region, are shown by the dash-dotted trace. A visible narrowing of the simulated photoelectron line occurs, but the ensuing improvement in energy resolution is not better than 20%. A much more significant narrowing occurs when only emission of electrons into the half-sphere on the detector side is allowed, see the dash-dot-dot-dotted trace. The electrons which travel in the opposite direction before being turned around by the strong magnetic field will have slightly longer flight times. We thus conclude that the exact configuration of the magnetic field and the interaction region does not have a large influence on the energy resolution of the spectrometer, as long as electrons emitted into the full solid angle are accepted. Going back to the original magnetic bottle configuration with 2π sr acceptance would improve resolution, but would be hard to achieve with the arrangement of magnets chosen in our design.

In the original Kruit and Read design of the magnetic bottle spectrometer, the interaction region coincided with the maximum strength of the collecting magnetic field.[4] In our modified design according to Cheshnovsky[10] this is no longer the case, and since the *B*-field is maximal at the surface of the magnet tip it is not even possible. The question therefore arises as to what extent the exact position of the magnet tip influences the count rate, resolution, and signal to noise ratio of the electron spectra. We found that the spectrum is not influenced much by moving the magnet by 1–2 mm in the plane perpendicular to the spectrometer axis.

On the other hand, moving the magnet tip along the spectrometer axis (z axis) has a considerable influence. In Fig. 3, three representative He 1*s* spectra are shown. The one drawn by a solid curve was recorded with the magnet being as close as possible to the interaction region, whereas for the others the magnet was retracted in the negative *z* direction. The spectra look clearly different: Whereas in the first case a sharp peak can be observed, retracting the magnet leads to a rise in intensity but also to a broadening of the line. Between the solid line and the dashed line spectra, the observed full width at half maximum (FWHM) of the time-of-flight spectra increases from 7.8 to 8.7 ns. A constant contribution of the monochromator broadening has also to be taken into account when assessing the amount of broadening. We discuss this below.

A series of spectra at various distances between the magnet tip and the interaction region has been measured. The areas of the He 1*s* peak have been plotted in Fig. 4, together with the total counts of each measurement. In contrast to the total count rate which increases when the magnet is withdrawn, the data suggest the existence of an optimal position for which the number of counts in the actual peak is at a maximum.

In principle, two effects can play a role in the explanation of the observed *z*-dependent behaviour: 1. The size of the "loss cone" of emission in the direction of the magnet, for which the component parallel to the field lines is too strong to be turned around, depends on the *z*-position of the source point. 2. The effective interaction region might become larger

when the magnet is retracted, because the magnetic field very near to the tip is well confined.

The opening angle of the loss cone is well known from the treatment of magnetic mirror machines, which are used for plasma confinement.[3] For particles created on the rotation axis it reads

$$|v_{\parallel}| < |v_{\perp}| \sqrt{B_{max}/B_z(0) - 1}, \quad (1)$$

where $v_{\parallel}$ and $v_{\perp}$ are the particle velocities parallel and perpendicular to the magnetic field lines, B_{max} the maximum absolute value of the B-field and $B_z(0)$ its value at the source point.[3] While Eq. (1) indicates that the loss cone generally decreases when the magnet is moved away from the interaction (z becomes more negative, $B_z(0)$ becomes smaller), in this particular example it is unclear whether the measured data can be explained from this fact. This is because the angular variation of photoelectron intensity after photoionization by linearly polarized light can be written as

$$f(\vartheta) = 1 + \frac{\beta}{4}(1 + 3p\ \cos 2\vartheta)). \quad (2)$$

Here, β is the so-called angular distribution parameter, which contains the influence of the quantum mechanical transition amplitudes, p is the degree of linear polarization (Stokes parameter), and ϑ the angle relative to the polarization axis. Approximately, this axis lies in the storage ring plane, that is $\perp$ to the z direction. For He 1s photoelectrons, β has a value of 2, which leads to a vanishing emission probability along the z direction. Therefore in this particular case, not much is gained if more electrons from within a cone aligning with the z axis can be accepted. In other words, in the chosen geometry and for the chosen system our set-up is not very sensitive to changes of the size of the loss cone. We note that this is not a general property, since only photoelectron lines from s-like atomic orbitals are so strongly anisotropic.

Time-of-flight differences between photoelectrons emitted into the forward and backward directions are readily apparent in our experiment when photoelectrons from s-like orbitals are observed with light polarized linearly along the spectrometer axis. In such cases, the time-of-flight spectrum shows two sharp peaks with a local minimum in-between. In the spectrum shown here, due to the different geometry these "forward" and "backward" peaks are not apparent. However, we believe that also in our case the spectral broadening which is observed at more negative z-values of the magnet results from the increasing difference in pathlength between trajectories turned around by the magnetic mirror, and those emitted "directly."

Towards more negative z-values also a strong background starts to appear in the spectra. Already for $z = -1.75$ mm the background of scattered electrons appearing at the low energy side of the He 1s peak is significantly larger than for $z = -1.1$ mm, which might become important when detection of weak signals is desired. Scattered electrons in our spectrometer are significant at all values of z, but as they are distributed over a large range of time channels it was not possible to quantify them.

We therefore arrived at the following, speculative explanation for Figs. 3 and 4: At the position of maximal He 1s signal the volume probed equals the volume of the interaction region, i.e., the volume defined by the overlap between gas jet and synchrotron radiation. Moving the magnet closer to the interaction region reduces the size of the interaction volume probed and thus decreases the count rate. Retracting the magnet instead increases the volume probed, but since the size of the interaction region is fixed, this most likely only adds background counts, leading to the observed difference between total counts and peak intensity.

All measurements shown below were recorded at small absolute values of the magnet z position (between -1.2 and -1.5 mm).

B. Energy resolution

To determine the energy resolution of the spectrometer, He 1s and Ar $3p_{3/2}$ photoelectron spectra have been recorded for a series of photon energies, covering the range from the ionization threshold up to 11 eV above. The linewidth, measured as the FWHM of the peaks after time-to-energy conversion, is plotted vs. kinetic energy (open circles) in Fig. 5. For the Ar spectra, the width has been determined from a fit of two Gaussian profiles to the Ar $3p$ fine structure components. Non-Gaussian peak shapes are observed for these lines towards the higher kinetic energies of our measurements, but visual inspection of our fitted profiles shows that they nevertheless agreeably represent the total line broadening.

The observed widths result from a combination of the analyzer resolution and the monochromator broadening. Both quantities are *a priori* unknown. We assumed for the total broadening $w = \sqrt{w_m^2 + w_a^2}$, with $w_{m,a}$ the contributions of monochromator and analyzer, respectively. To determine w_a, we have required the contribution of the monochromator

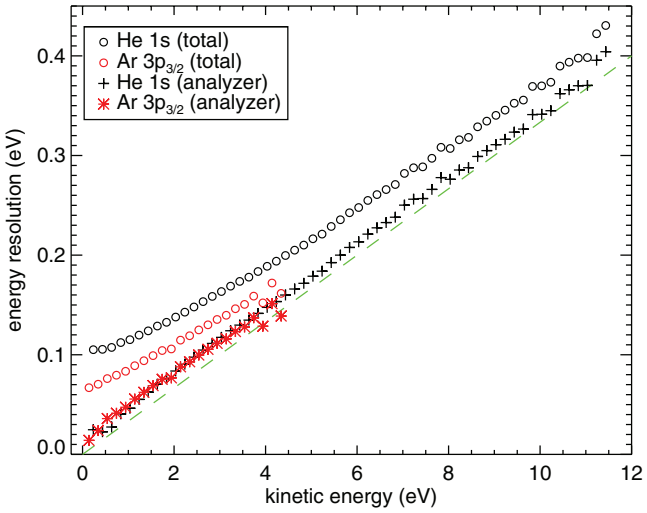

FIG. 5. Energy resolution (FWHM) of the spectrometer as a function of kinetic energy. Measurements of the atomic He 1s and Ar $3p_{3/2}$ photoelectron lines were analysed. Open circles show the total apparatus broadening, including spectrometer and monochromator contributions. The "pluses" and "asterisks" show the values after subtraction of an approximate monochromator broadening, see text for details. The dashed line shows the expected broadening for a spectrometer with a resolving power of $E_{kin}/\Delta E_{kin} = 30$. An acceleration voltage of +1.1 V was applied to the drift tube and the entrance aperture of the spectrometer.

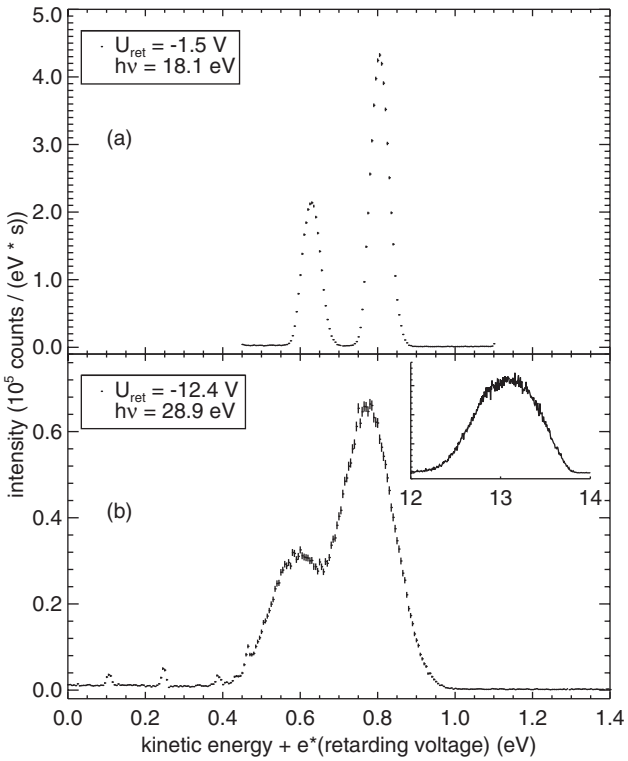

FIG. 6. Photoelectron lines for the Ar $3p_{3/2}$ and $3p_{1/2}$ levels showing the effect of applying a retardation voltage U_{ret}. The retardation voltage (a negative number) has been added to the original kinetic energy of the photoelectrons so that the doublet occurs at the same place in each panel. Intensity is given as 10^5 counts per unit energy interval and second. The inset to panel (b) shows a spectrum taken (vs. kinetic energy) at the same photon energy (28.9 eV), but without any retardation.

to be a constant fraction of the photon energy ($h\nu/w_m(h\nu)$ = const.). This unknown constant was then determined such that for both series of photoelectron lines, recorded at identical kinetic energies but different photon energy, the values of the analyzer contribution to the broadening, w_a, coincided. (The result for w_m was $h\nu/w_m(h\nu) \approx 240$, in accordance with expectations for the TGM4 beamline.) In this terminology, open circles in Fig. 5 show w, and other symbols show w_a for He and Ar (drawn as + and *). The peak widths increase linearly with the energy of the electrons, as previously observed for other time-of-flight spectrometers.[23] The resolving power $E/\Delta E$ of our analyzer determined from these data increases from about 22 for $E = 1$ eV to about 29 for $E = 10$ eV. (E: kinetic energy; we note that w_m is much smaller for the data in Fig. 2, as they were recorded on another beamline.)

The energy resolution of the spectrometer can be improved by applying a deceleration voltage to the drift tube. This is demonstrated for the Ar $3p$ photoelectron spectrum in Fig. 6. In the top panel, a photon energy of 18.1 eV was used for ionization, and a retardation voltage of −1.5 V was applied. The spin-orbit splitting of 180 meV between the two $3p$ components can easily be resolved. For the spectra shown in the bottom panel, the photon energy was increased to 28.9 eV. Without any retardation, one obtains the spectrum shown in the inset, which merely shows a broad peak around 13 eV kinetic energy. A retardation voltage of −12.4 V is then applied to the entrance aperture and the drift tube, which reduces the kinetic energy of the electrons inside the drift tube to the same value they had in the panel (a) spectrum. The fine structure components are now separated, but not to the same extent as in the low photon energy spectrum. A possible reason for this could lie in the fact that the electron is created with a higher kinetic energy, and only later slowed down. A faster electron which is emitted perpendicular to the spectrometer axis or towards the magnet will travel a longer distance before its movement is parallelized to the field lines than a slower one, for which less energy has to be overcome. Taking into account that the monochromator broadening is also larger in the bottom panel, we find that the analyzer resolution for the strongly retarded spectrum is around 120 meV, which corresponds to a $E/\Delta E$ of 110, where E is the unretarded kinetic energy.

C. Transmission and detection efficiency

Another important characteristic of an electron spectrometer is its transmission. In order to gain information on transmission properties, we have analyzed series of Ar $3p$ and He $1s$ spectra. Photon energies were scanned in steps of 0.2 eV from below the corresponding ionization thresholds to 5 eV above. For each step, a time-of-flight spectrum was recorded. The Ar $3p_{3/2}$ and $3p_{1/2}$ peaks, and the He $1s$ peak were identified and the peak areas determined. Values obtained such were corrected for the corresponding ionization cross sections,[30] the decrease of the synchrotron radiation intensity during the scan and the photon energy dependence of the beamline flux. The resulting figures represent the detection efficiency of the spectrometer up to a fixed, but unknown factor, to which the sample gas density in the interaction region and the size of the latter, weighted by the respective solid angle, contribute. They are shown in Fig. 7. Also included in this graph is a trace

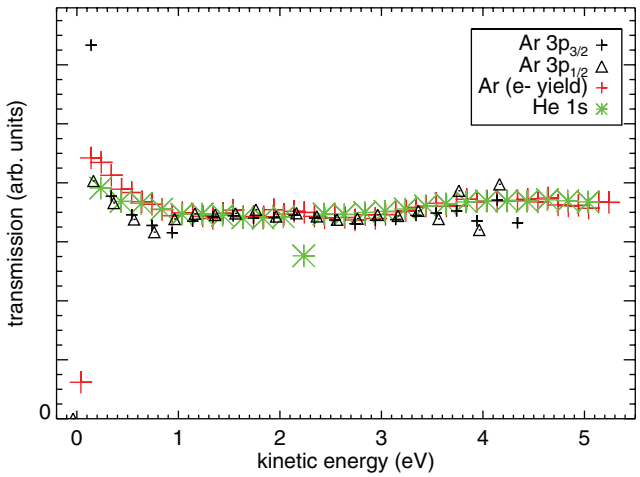

FIG. 7. Intensity of the Ar $3p_{3/2}$ and $3p_{1/2}$ photolines normalized to the ionization cross section, ring current, and the flux curve of the beamline. Resulting values reflect the kinetic energy dependence of the spectrometer transmission function, on an arbitrary scale. The lowest Ar $3p_{3/2}$ data point (E_{kin} = 0.12 eV) is supposedly influenced by autoionization of Ar $3p_{1/2}^{-1}nl$ Rydberg states. For comparison, values from a total electron yield measurement on Ar and from measuring the He $1s$ photoline are shown. The latter two data sets were scaled to the average value of the Ar $3p_{3/2}$ data. An acceleration voltage of +1.1 V was applied to the drift tube and the entrance aperture of the spectrometer.

from a total electron yield measurement of Ar (pluses). The transmission function is flat. The slight increase for kinetic energies below one eV might be caused by field penetration through the aperture of the drift tube. The lowest kinetic energy at which electrons are observed for +1 V acceleration is below 25 meV.

An oscillation of the transmission function vs. kinetic energy was seen with the instrument when a too low value of the guiding field (0.25 mT) was set. Based on our simulations, we interpret this behavior as a side effect of a non-adiabatic drop in the magnetic field under these conditions. If the field drops too rapidly, trajectories may develop "in-phase" nodes and anti-nodes due to the cyclotron motion around the field lines (see Ref. 4). In our instrument, this may lead to a kinetic energy-dependent loss of electrons at the entrance aperture.

Furthermore, the transmission function has been studied with accelerating and retarding voltages applied to the drift tube. Several settings were probed by recording the Ar $3p_{3/2}$ photoelectron line at a number of photon energies $h\nu_i$, which were determined such that for every retardation voltage U_{ret}, the set of retarded kinetic energies $\{h\nu_i - E_b + eU_{ret}\}$ was the same (with E_b the ionization potential as given above). To determine the areas of only the Ar $3p_{3/2}$ peaks, Gaussian line profiles were fitted to the data. These represented the peak area sufficiently well, although the line profiles of the magnetic bottle are not necessarily of Gaussian shape. The peak areas were then corrected in the same manner as for the previous figure and plotted versus the initial kinetic energy of the electron, i.e., before retardation or acceleration (Fig. 8).

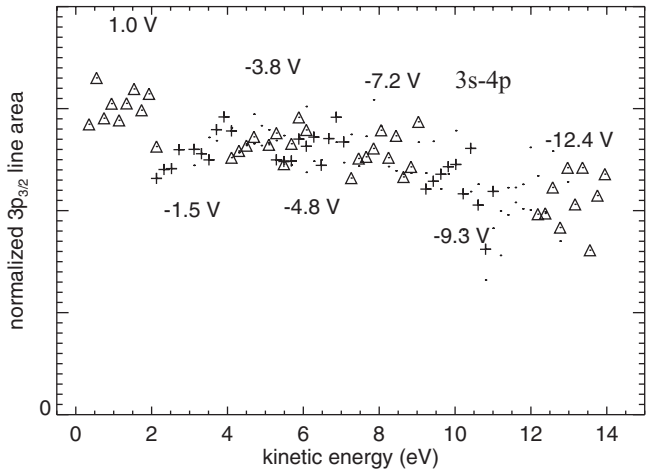

FIG. 8. Intensity of the Ar $3p_{3/2}$ photoline normalized to the ionization cross section, ring current, and beamline flux. Data points for different settings of the retardation voltage are shown, and for each setting a number of measurements within a kinetic energy interval of 2 eV width. In total, the resulting values reflect the kinetic energy dependence of the spectrometer transmission function, on an arbitrary scale. Data points are shown for an acceleration/retardation voltage of +1, −3.75, −7.2, −12.4 V (triangles, from left to right) and −1.5, −4.8, −9.3 V (crosses). Additional data points at intermediate settings of the retardation voltage are shown by dots. The 3*p* fine structure components were separated by fitting Gaussian line profiles to the data. See text for details. The influence of the Ar $3s \rightarrow 4p$ window resonance[36] is seen at kinetic energies around 10 eV.

For each particular retardation voltage there seems to be a tendency for the transmission to increase as a function of kinetic energy, but the effect is only in the range of ±10%. Values from spectra recorded at other retardation voltages fit well to the series, presenting an overall smooth behavior of the spectrometer under retardation conditions. The poorer stability of the data points at high absolute values of the retardation is the result of strongly non-Gaussian peak profiles, which led to a worse fidelity of our peak fits. The influence of the Ar $3s$–$4p$ window resonance[36] can be seen at about 10 eV kinetic energy. The essence of Fig. 8 is that retardation by more than 80% of the initial kinetic energy can be used without impairing the transmission by much.

The relative stability (within 10%) of the transmission of our instrument using electrostatic retardation is not a trivial result, because electrons may overcome an electrostatic barrier of height $(-eU_{ret})$ only, if the kinetic energy of their velocity component *in the direction of the electric field* is larger than the barrier height.[4] That is, in the absence of parallelization, a substantial drop of the transmission function is expected. Our results seem to say that parallelization in our instrument occurs "quicker" than the increase of electric potential between the point of interaction and the drift tube.

The careful reader will note that for some data points in Fig. 8 the kinetic energy E is below the product of $-e$ times the retarding voltage. U_{ret} was applied to aperture and drift tube, while keeping the mesh at ground potential. The interaction region therefore is on a small bias potential as it is close to, but not coincident with the mesh. This might produce the observed effect. In any case its occurrence does not alter our conclusions about the spectrometer.

So far, our discussion of the transmission function was based on values in arbitrary units. An absolute figure for the detection efficiency of the spectrometer is also of great interest, e.g., for count rate estimates on ultra-dilute targets, and for coincidence experiments. We have determined this figure by analyzing electron spectra after Xe 4*d* photoionization. The 4*d* levels show a large spin-orbit splitting, and decay by Auger emission. The probability for detecting a $4d_j$ photoelectron in coincidence to a pertaining Auger electron can be written as $p(4d_j)p(Au)b(Au)$, where $p(-)$ are the respective detection probabilities and b the branching ratio of the Auger line which is considered for the analysis. We assume $p(4d_j) = p(Au)$ because our transmission function is flat. The Auger transitions at 8.3 and 10.3 eV were used. Line areas proportional to $p(4d_j)$ and $p(Au)b(Au)$ can be read from a one-dimensional histogram of our event files (the conventional electron spectrum, such as the one shown in Fig. 2), while an area proportional to $p(4d_j)p(Au)b(Au)$ was read from a two-dimensional histogram of all electron pairs received, with their times-of-flight as the independent axes. The branching ratios were calculated from the relative Auger intensities in Table 1 of Ref. 31, and were corrected for the contribution of double Auger decay not taken into account there (18% for $j = 5/2$ and 24% for $j = 3/2$, Ref. 32). Corrected numbers were $b(Au^{3/2}) = 0.14$ (Auger electron pertaining to $j = 3/2$) and $b(Au^{5/2}) = 0.16$. Values for the detection efficiency arrived at by this exercise are around $0.6^{+0.05}_{-0.1}$ for $p(4d_{5/2})$, $p(4d_{3/2})$, and $p(Au^{3/2})$. For two measurements of $p(Au^{5/2})$, lower

values around 0.4 were found, for a reason yet unknown. These discrepancies will be investigated in a later study.

IV. DISCUSSION AND SUMMARY

In this article, we have described our version of a short magnetic bottle electron spectrometer, dedicated to experiments at synchrotron radiation sources, where VUV radiation with a high repetition rate is emitted, and slow photoelectrons are produced. A number of properties of the spectrometer have been experimentally demonstrated, which are of relevance for electron spectroscopy on gas phase species, e.g., a molecular or cluster jet. In particular, we would like to mention characteristics such as the flat transmission function, which is still maintained even on application of a high retardation voltage, as well as the energy resolution and the possibility of increasing it by electrostatic retardation.

We were able to simulate the lineshape of our analyzer by a conventional ray-tracing program. These simulations present evidence that the size of the interaction region, which inevitably is extended along the photon beam in synchrotron radiation studies of gaseous species, is less important for the energy resolution than solid angle effects. In the example we have considered, the original Kruit and Read design of the magnetic bottle spectrometer (2π sr acceptance) had roughly a factor two better energy resolution than the modified design with almost 4π sr, which is used in later instruments.

The large acceptance angle and the good transmission—also at low kinetic energies—make this kind of spectrometer superior to conventional electrostatic analyzers when multi-electron coincidences are to be investigated. The spectrometer has been successfully employed in coincidence experiments on low-energy electrons arising from non-local autoionization processes in rare gas clusters.[33–35]

ACKNOWLEDGMENTS

Financial support from the Fonds der Chemischen Industrie, the Advanced Study Group of the Max Planck Society, and the German Research Foundation (DFG) is gratefully acknowledged. M.M. and T.L. wish to thank Andreas Gaupp from BESSY II for useful discussion on permanent magnets. The help of Hans-Peter Rust with data acquisition and of Simon Weisemann with magnetic field measurements is gratefully acknowledged. Thanks are due to Jens Viefhaus for comments on the probability of double Auger decay. We acknowledge the Helmholtz-Berlin for the allocation of synchrotron radiation beamtime.

[1]R. Dörner, V. Mergel, O. Jagutzki, L. Spielberger, J. Ullrich, R. Moshammer, and H. Schmidt-Böcking, Phys. Rep. **330**, 95 (2000).
[2]A. T. J. B. Eppink and D. H. Parker, Rev. Sci. Instrum. **68**, 3477 (1997).
[3]R. J. Goldston and P. H. Rutherford, *Introduction to Plasma Physics* (Taylor and Francis, 1995).
[4]P. Kruit and F. H. Read, J. Phys. E **16**, 313 (1983).
[5]U. Hergenhahn, J. Electron Spectrosc. Relat. Phenom. **184**, 78 (2011).
[6]M. Förstel, M. Mucke, T. Arion, T. Lischke, S. Barth, V. Ulrich, G. Öhrwall, O. Björneholm, U. Hergenhahn, and A. M. Bradshaw, Phys. Rev. B **82**, 125450 (2010).
[7]P. Kruit, M. J. van der Wiel, and F. H. Read, AIP Conf. Proc. **90**, 390 (1982).
[8]T. Tsuboi, E. Y. Xu, Y. K. Bae, and K. T. Gillen, Rev. Sci. Instrum. **59**, 1357 (1988).
[9]G. Beamson, H. Q. Porter, and D. W. Turner, Nature (London) **290**, 556 (1981).
[10]O. Cheshnovsky, S. H. Yang, C. L. Pettiette, M. J. Craycraft, and R. E. Smalley, Rev. Sci. Instrum. **58**, 2131 (1987).
[11]J. H. D. Eland, O. Vieuxmaire, T. Kinugawa, P. Lablanquie, R. I. Hall, and F. Penent, Phys. Rev. Lett. **90**, 053003 (2003).
[12]F. Penent, P. Lablanquie, R. Hall, J. Palaudoux, K. Ito, Y. Hikosaka, T. Aoto, and J. Eland, J. Electron Spectrosc. Relat. Phenom. **144–147**, 7 (2005).
[13]P. Lablanquie, T. P. Grozdanov, M. Žitnik, S. Carniato, P. Selles, L. Andric, J. Palaudoux, F. Penent, H. Iwayama, E. Shigemasa, Y. Hikosaka, K. Soejima, K. Nakano, I. H. Suzuki, and K. Ito, Phys. Rev. Lett. **107**, 193004 (2011).
[14]S. Lochbrunner, J. J. Larsen, J. P. Shaffer, M. Schmitt, T. Schultz, J. G. Underwood, and A. Stolow, J. Electron Spectrosc. Relat. Phenom. **112**, 183 (2000).
[15]S. Douin, J.-H. Fillion, M. Bonneau, P. Bréchignac, D. Furio, D. Gauyacq, M. Horani, and N. Shafizadeh, Chem. Phys. Lett. **216**, 215 (1993).
[16]C. Lüder and K. H. Meiwes-Broer, Chem. Phys. Lett. **294**, 391 (1998).
[17]K. L. J. Knappenberger, C. E. J. Jones, M. A. Sobhy, and A. W. J. Castleman, Rev. Sci. Instrum. **77**, 123901 (2006).
[18]H. Handschuh, G. Ganteför, and W. Eberhardt, Rev. Sci. Instrum. **66**, 3838 (1995).
[19]F. Buchner, A. Lübcke, N. Heine, and T. Schultz, Rev. Sci. Instrum. **81**, 113107 (2010).
[20]T. Ohdaira, R. Suzuki, T. Mikado, H. Ohgaki, M. Chiwaki, and T. Yamazaki, Appl. Surf. Sci. **116**, 177 (1997).
[21]M. Meyer, J. T. Costello, S. Düsterer, W. B. Li, and P. Radcliffe, J. Phys. B **43**, 194006 (2010).
[22]C. Domesle, B. Jordon-Thaden, L. Lammich, M. Förstel, U. Hergenhahn, A. Wolf, and H. B. Pedersen, Phys. Rev. A **82**, 033402 (2010).
[23]P. Lablanquie, L. Andric, J. Palaudoux, U. Becker, M. Braune, J. Viefhaus, J. Eland, and F. Penent, J. Electron Spectrosc. Relat. Phenom. **156–158**, 51 (2007).
[24]O. Hemmers, S. B. Whitfield, P. Glans, H. Wang, D. W. Lindle, R. Wehlitz, and I. A. Sellin, Rev. Sci. Instrum. **69**, 3809 (1998).
[25]M. Mucke, "Employing electron-electron coincidence techniques to investigate the autoionisation of clusters," Ph.D. dissertation (Technical University Berlin, 2011), see http://opus.kobv.de/tuberlin/volltexte/2011/3073/ Ph.D. thesis.
[26]S. P. Marburger, O. Kugeler, and U. Hergenhahn, AIP Conf. Proc. **705**, 1114 (2004).
[27]Simion 8.0, (c) 2003–2011 Scientific Instrument Services, Inc. (SIS), http://simion.com, primary author version 8.1/8.0/SL David J. Manura, SIS.
[28]J. C. Slater and N. H. Frank, *Electromagnetism* (Dover, 1969), p. 58.
[29]M. Förstel, Ph.D. thesis, to be published.
[30]J. A. R. Samson and W. C. Stolte, J. Electron Spectrosc. Relat. Phenom. **123**, 265 (2002).
[31]A. Kivimäki, L. Pfeiffer, H. Aksela, E. Nõmmiste, and S. Aksela, J. Electron Spectrosc. Relat. Phenom. **101–103**, 43 (1999).
[32]N. Saito and I. H. Suzuki, J. Phys. Soc. Jpn. **66**, 1979 (1997).
[33]M. Mucke *et al.*, to be published.
[34]M. Förstel, M. Mucke, T. Arion, A. M. Bradshaw, and U. Hergenhahn, Phys. Rev. Lett. **106**, 33402 (2011).
[35]T. Arion, M. Mucke, M. Förstel, A. M. Bradshaw, and U. Hergenhahn, J. Chem. Phys. **134**, 074306 (2011).
[36]A. Svensson, M. O. Krause, and T. A. Carlson, J. Phys. B **20**, L271 (1987).